Front. Energy 2022, 16(6): 883–899
https://doi.org/10.1007/s11708-021-0770-z

REVIEW ARTICLE

Hecong LIU, Weiwei CAI

Recent progress in electric-field assisted combustion: a brief review

Abstract The control of combustion is a hot and classical topic. Among the combustion technologies, electric-field assisted combustion is an advanced technology that enjoys major advantages such as fast response and low power consumption compared with thermal power. However, its fundamental principle and impacts on the flames are complicated due to the coupling between physics, chemistry, and electromagnetics. In the last two decades, tremendous efforts have been made to understand electric-field assisted combustion. New observations have been reported based on different combustion systems and improved diagnostics. The main impacts, including flame stabilization, emission reduction, and flame propagation, have been revealed by both simulative and experimental studies. These findings significantly facilitate the application of electric-field assisted combustion. This brief review is intended to provide a comprehensive overview of the recent progress of this combustion technology and further point out research opportunities worth investigation.

Keywords electric field, combustion, flame stabilization, emission reduction, flame propagation

1 Introduction

Combustion represents a complicated physical and chemical process, typically accompanied by the intense release of heat and radiation, which are collected and utilized for energy production and to serve mundane life. The majority of energy resources empowering the modern society were converted through the combustion of fossil fuels and this situation will continue for several decades in the future [1,2]. Countless applications of combustion were developed, e.g., providing thrust for engines and energy source for power plants, etc. With the rapid development of modern society, more stringent requirements were proposed for combustion devices such as lower emission and better stabilization under harsh environments. To suffice these requirements, many attempts were devoted to developing advanced combustion systems and technologies. For instance, homogeneous charge compression ignition (HCCI) with a high compression ratio and a low temperature was proposed to increase the combustion efficiency and reduce the NO_x emission of internal combustion engines [3]. Besides, the lean premixed combustion technology was also developed to decrease the emission of gas turbine engines [4]. Moreover, rotating detonation was developed to increase the thrust-weight ratio of rocket engines [5].

Among the emerging combustion techniques, electric-field assisted combustion (EFAC) is a promising one. The interaction between the flame and the external electric field was first reported by Brande in 1814 [6]. In his demonstration, different kinds of flames placed between two electrodes were found to be bent toward different electrodes, accompanied by the increase of temperature. For example, the flame of potassium and camphor were drawn to the positive electrode, while the flame of phosphorus was attracted by the negative electrodes. This phenomenon was attributed to the charged particles in the flames. Since the observation of Brande, the impacts in multiple aspects of the electric field on combustion have been expounded, including emission reduction [7], flame stabilization [8], and flame propagation [9]. More specifically, the electric field can reduce emissions, e.g., CO, increase the blow-off velocity which can extend the limit of the lean premixed combustion technology. Besides, the EFAC features fast response and low power consumption. It was reported that the power consumption in the sub-saturation region was around 0.01% of the thermal power [7]. It is, therefore, reasonable to believe that EFAC could be a good remedy to cover some

Received Dec. 22, 2020; accepted Apr. 4, 2021; online Sept. 30, 2021

Hecong LIU, Weiwei CAI (✉)
Key Laboratory of the Ministry of Education for Power Machinery and Engineering, School of Mechanical Engineering, Shanghai Jiao Tong University, Shanghai 200240, China
E-mail: cweiwei@sjtu.edu.cn

drawbacks of combustion systems. The electric characteristics of the flames are widely investigated as well. However, compared with normal combustion, the fundamental principle of combustion under an electric field is much more complicated. To better understand the coupling between physical, chemical, and electromagnetic processes, experimental, numerical, and theoretical studies were conducted. Among the various studies, a critical point is to acquire the spatiotemporal measurements of flame physical quantities such as temperature, pressure, and velocity by advanced diagnostics, e.g., non-intrusive optical techniques [10]. The acquired information reveals the nature of the flame and can support the validation of simulation models and the optimization of practical combustors.

A similar concept to EFAC is plasma-assisted combustion (PAC) which is also a hot topic in combustion research. The key point of PAC is to generate plasma. Up to the present, various methods have been proposed, e.g., dielectric barrier discharge [11], microwave [12], laser [13], and so on, of which, the electric field is a common approach. The difference between EFAC and PAC with electric field is that the electric field strength for EFAC is much weaker and no corona can be found. Therefore, no plasma is generated. The typical electric field strength can be larger than 10^{10} V/m for PAC [14], while it is around 10^5 V/m for EFAC [15,16]. It was also reported that the power for PAC, e.g., corona, was 500 times greater than that for EFAC in the sub-saturation region [17]. PAC was summarized by Ju and Sun [14]. Hence, this work only focuses on EFAC where no plasmas is generated.

Three reviews on the electrical aspect of combustion [18], ignition and combustion process under electric field [19], and ions in the flames [20] respectively were published in the last century. These reviews provide an excellent overview of EFAC. However, due to the lack of advanced diagnostics, more detailed phenomena and explanations are missing in these reviews. Thanks to the recent progress in diagnostics and the combustion system, more comprehensive mechanisms are proposed to explain the complicated phenomena induced by the electric field. Thus, it is a proper time to provide the readers with a comprehensive introduction into recent progresses, especially those in the last two decades, with the intention to discuss the fundamental mechanisms of the EFAC, review the electrical characteristics of the flame, present and explain the electric-field-induced phenomena, and discuss the opportunities and challenges in the future.

2 Electric-field assisted combustion mechanisms

During the combustion process, numerous charged particles, i.e., ions and electrons are generated in pairs due to thermal ionization, excitation, and chemi-ionization [21,22]. Among the above mechanisms, chemi-ionization is believed to be dominant for the formation of ions [23]. In hydrocarbon flames, the most likely positive particles are H_3O^+, CH_3^+, and CHO^+, while the negative ions are O_2^-, OH^- and O^- [24]. The negative ions are unstable at high temperatures and quickly decay to electrons and neutral particles [7]. Hence, most negative charges are carried by electrons. The concentration of the positive ions can be up to 10^9–10^{12} ions/cm^3 within the reaction zone of the premixed flame. Since the flame keeps the electric neutrality as a whole, the concentration of negative ions is much less than that of positive ions. The flame can be considered as a low-temperature plasma [25]. The impacts of the electric field on the flame can be attributed to three effects, i.e., the ionic wind effect or the electro-hydrodynamic effect, the chemical effect, and the Joule heat effect [19].

The proposal of the ionic wind effect can be dated back to the 1900s [26,27]. The ionic wind effect can explain most electric-field-induced phenomena, e.g., the generation of forced convection in the absence of gravity [28] and the alternation of the flame shape [15]. The dominant effect has been validated on co-flow flames and candle type flames by simulation [29]. Figure 1 is an illustration of the ionic wind in the one-dimensional model. When the electric field is imposed, the charged particles will accelerate and flow toward the oppositely charged electrodes due to the effect of the Lorentz force. More specifically, the positive particles will move to the negative electrode, while the negative particles will migrate to the positive electrode. The drift velocity of the accelerated ions can be expressed as $v_d = \mu E$, where μ is the mobility of the particles and E represents the electric field strength [24]. As for the electron, the mobility is reported to be 0.4 m^2/(V·s) in the reaction zone and burnt region of a

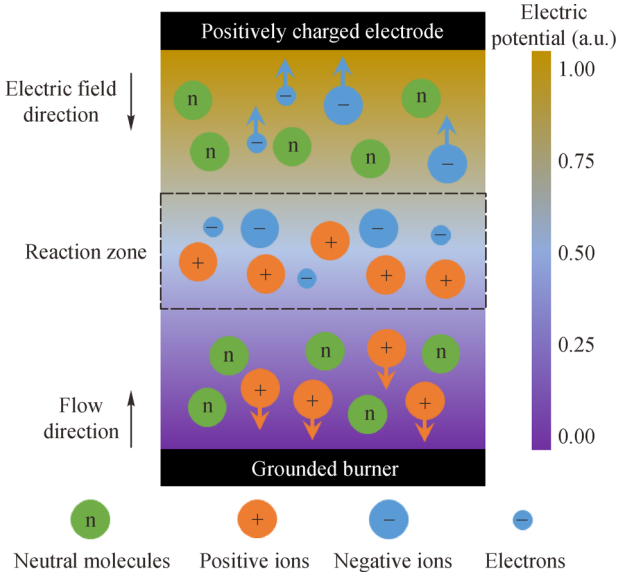

Fig. 1 Illustration of ionic wind.

premixed flame, independent of equivalence ratio [30]. A more accurate estimation of drift velocity for electron has been proposed as $v_e = \sqrt{\mu_a E} + \mu_b E$, where μ_a and μ_b can be obtained through simulation [31]. Before the charged particles hit the electrodes, a number of random collisions will happen between the accelerated charged and neutral particles within the mean free path. The collisions can transfer the momentum, change the velocity of the neutral particles, and finally modify the bulk flow. Due to the low concentration of the negative ions and the small momentum carried by the electrons, it is reasonable to ignore the influence of negative ions and electrons in most cases. The maximum ionic wind velocity is theoretically proportional to the electric field strength, expressed as $v_{ionic} = E/\sqrt{8\pi\rho}$, where ρ is the gas density [21,32]. It is well-recognized that there is a response time before the ionic wind leads to the significant influence. Kono et al. [33] proposed a theoretical response time based on the collision theory $t_c = 1/(zR_i)$, where z is collision frequency, R_i is the ratio of ions to neutral particles. The flow field can respond faster than the flame shape [34]. Up to date, the response times based on different observations have been reported from 2 ms to 36 ms [35–37]. To better understand the response of ionic wind, the so-called developing degree of ionic wind was also proposed, defined as $\xi = 1 - \exp(1 - t/t_c)$, where t is the time after imposing the electric field and t_c is collision response time. Recently, a non-monotonic phenomenon between frequency and blow-off velocity was observed by Kim et al. which cannot be explained by the sole migration of positive ions. To address this problem, the so-called bi-ionic wind effect was proposed [38]. In this theory, electrons can collide with O_2 and H_2O to generate negative ions, i.e., O_2^-. The existence of these negative ions can significantly influence the behavior of the flames as well, and the developing degree of ionic wind is then modified as $\xi_{eff} = \xi_{positive} - \eta\xi_{negative}$, where η is the ratio between negative and positive ions, and $\xi_{positive}$ and $\xi_{negative}$ are the developing degree for positive ions and negative ions, respectively. The simulation has confirmed that the negative ions can play a crucial role [39] and reproduced the three-dimensional flow structure induced by the bi-ionic wind [40]. A typical developing degree curve of bi-ionic wind is shown in Fig. 2, which indicates that the curve has a local maximum at an alternating current (AC) frequency of near 10 Hz. Besides, the ionic wind can further induce the pressure drop across the flame which is around 40.53 Pa [35]. However, if the electrodes and the flames couple more closely, the pressure difference may become large enough to change the flame shape, which is called the electric pressure effect [35].

The chemical effect is the direct action of the electric field on the chemical reaction. The charged particles are accelerated under the electric field, hence, the particles carry high energy and can directly enhance the chemical reaction rate [38]. Besides, the accelerated electrons may collide with N_2 and excite N_2. The excited N_2 will transfer the energy to other molecules, e.g., O_2. The excited O_2 will increase the reaction rate as well [19].

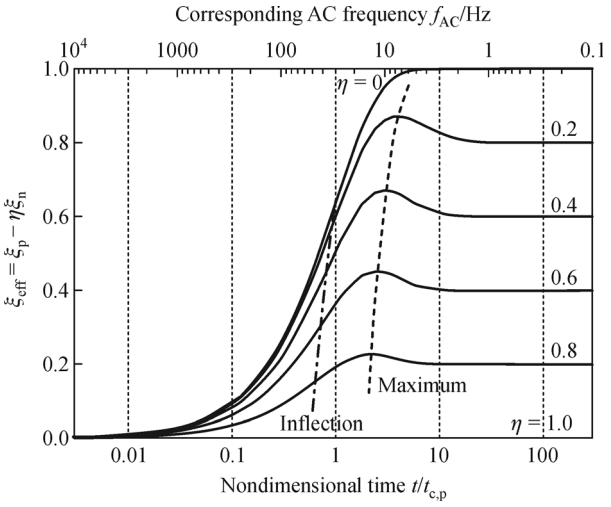

Fig. 2 Effective developing degree curve of bi-ionic wind (adapted with permission from Ref. [38]).

The electric field can generate heat to influence the flame as well, which is referred to as the Joule heat effect. The generated heat can increase the temperature of the flow and the reaction rate. On the one hand, the stable flames under electric heating have been reported by Chen et al. [41]. On the other hand, as reported by Marcum and Ganguly [35], the electrical power was not large enough to generate such high temperatures to modify the flame speed. Besides, the power of the electric field below breakthrough voltage is usually much smaller than that of the combustion system [7]. Thus, the Joule heat effect is always ignored.

3 Electrical characteristics

Since there are plenty of charged particles within the reaction zone, the flame will feature electrical characteristics [24]. When an electric field is imposed on the flame, the directional migration of the charged particles will lead to the current between the electrodes and the flame. The voltage-current characteristics (VCCs) have been extensively investigated based on different kinds of flames, e.g., jet flames and flat flames. Figure 3 plots the VCCs curves of flames under a direct current (DC) electric field. As the absolute values of the voltage and the current are dependent on the experimental conditions, e.g., flame type, Fig. 3 only demonstrates the trends of the VCCs and omits the values on the axes. Generally, there are three regions with different applied voltages [7,41–43]. Region 1 is called sub-saturation or recombination region, where positive ions and electrons can recombine to generate neutral particles while negative ions are resolved into

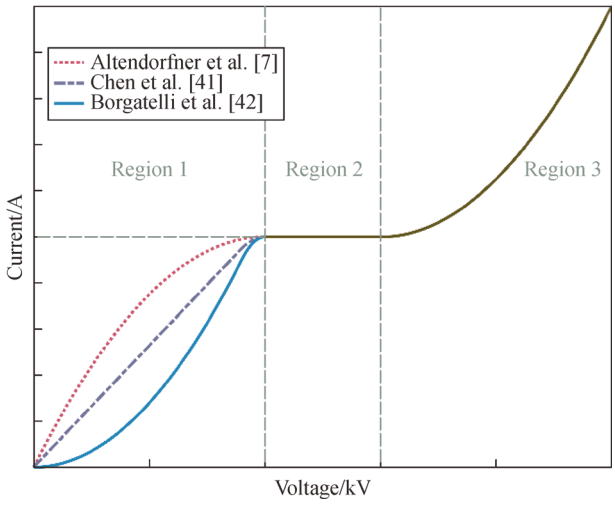

Fig. 3 VCCs curves under DC electric field (redrawn from Refs. [7,41,42]).

electrons and neutral particles. In Region 1, the current has a positive correlation with the applied voltage, which can be qualitatively attributed to the ionic wind effect. As shown in Fig. 3, three types of increasing curves are found. In the study conducted by Chen et al., the current increases linearly with the applied voltage [41]. However, other experiments show that the quadratic increasing curve is more common. Altendorfner et al. [7] and Borgatelli and Dunn-Rankin [42] observed two different quadratic curves as shown in Fig. 3. The difference between the slope of rising curves can be attributed to the position of the electrodes which leads to different resistances between the flame and the electrodes [44,45]. If reversing the direction of the DC electric field, i.e., the negative electrode is placed above the flame, the so-called diodic effect will appear, i.e., the current is dramatically decreased [15,35]. The diodic effect has been validated by the one-dimensional model [46]. This phenomenon is caused by the different mobilities of charged particles and the different travel distances before the charged particles hit the electrodes. In Region 2, the current is saturated and a higher applied voltage cannot increase the current anymore. In this region, all charged particles are removed from the reaction zone due to the electric field. The addition of other compounds, e.g., NaOH, can enlarge the saturation voltage and current due to the additional ions [47]. However, little research is conducted about the effects of additional compounds on other flame parameters under the electric field. Xiong et al. [48] developed an ionized layer model and successfully predicted the parabolic increase in the sub-saturation region and qualitatively explained the different functions of electrons and negative ions. The saturation current is dependent on the equivalence ratio [46]. Recently, it was reported that the saturated current was not affected by the pressure for lean and stoichiometric flames, while that for rich flames changed significantly due to the increase of pressure [49]. Region 3 is known as the super-saturation region. In this region, the applied voltage is larger than the breakthrough voltage, and more charged particles are generated due to the collisions between accelerated electrons and neutral particles. Hence, the current increases exponentially with the applied voltage [7]. Besides, the reaction rate and temperature in this region are enhanced due to the large ionic wind effect, which further increases the generation rate of the charged particles [42]. Based on the VCCs of the flame, Borgatelli and Dunn-Rankin [42] successfully demonstrated the active control of the electrical response of the flame in a high voltage circuit by using the proportional-integral-derivative method.

Apart from the typical VCCs, complicated curves are also observed on the other kinds of flames under various conditions [50–53]. Ren et al. [50] found two different VCCs by increasing and decreasing the voltage. When the voltage is increased, the current increases linearly first, and then quadratically. Further increasing the voltage leads to the dramatic rise of the current, accompanied by the change of the flame shape. When the voltage is decreasing, VCCs are completely different and the transition point is located much lower than that of increasing VCCs. Provided the AC electric field is applied, the VCCs manifest different behaviors compared with the DC electric field, which are more complicated. Chen et al. [41] tested the VCCs under an AC electric field as well and observed the parabolic increase of the current. Besides, the larger frequency can lead to a larger current. On the contrary, Park et al. [54] found the electric response of the counterflow flame to the AC electric field is more fluctuatory. When 10 Hz frequency was applied, a rapid increase was observed in the sub-saturation region. A higher frequency (larger than 100 Hz) can reduce the saturation current density due to the recombination of the charged particles.

4 Experimental design

To better understand the impacts of the electric field on the combustion process and the flame characteristics, dozens of experiments have been designed and conducted. The first example of the electric-field combustion setup was imposing the transverse DC electric field on the diffusion flame [6]. Since then, more representative premixed and diffusion flames with a wide range of electric fields have been extensively studied. The flame type includes jet flame [9,55,56], stagnation flame [50,57,58], counterflow flame [59,60], spherically expanding flame [23,61], and so on, while the electric fields include AC [36], continuous DC [62], pulsed DC [25,26] and high frequency (HF, larger than 1 kHz) voltage electric fields. Recently, a more complicated flame, i.e., swirl flame [7,16], was tested as well.

Typically, an EFAC system consists of an electric-field

supply system and a combustion system. The key component of the electric-field supply system is the high-voltage power supply. The output voltage of the power supply can be as high as 40 kV [7]. The high voltage is applied between the external electrodes and the burner, which is called double-electrode configuration. Recently, the so-called single-electrode configuration was proposed by Won et al. [55], which features a relatively lower power consumption compared to double-electrode configuration. In the single-electrode configuration, the burner is connected to the output terminal of the power supply while the ground is set as far as possible. Another important issue of the electric-field supply system is the selection of the electrodes. Up to the present, most electrodes are made of stainless steel due to its good electrical conductivity. However, the shapes of the electrodes can be quite different, including the ring shape, mesh shape, needle shape, plate shape, and so on. Therefore, it is necessary to estimate the distribution of the electric-field strength by theoretical derivation or simulation with commercial software, e.g., ANSOFT Maxwell [23]. According to the orientation between the electric field and the flame propagation, the electric field can be further divided into the transverse electric field [63] or the longitudinal electric field [55].

For the combustion system, the simplest burner adopted by the researchers is merely composed of a central tube with different diameters [65]. Figure 4 depicts other typical burners used in EFAC systems. The setup shown in Fig. 4(a) was designed to study the critical flow velocity of the co-flow jet flame, e.g., liftoff velocity, and frequently adopted by Won and the coworkers [9,55,56]. The co-flow burner consists of a central tube and a nozzle. The tube should be long enough to guarantee the full development of the flow profile. To prevent the influence of the ambient air, the uniform co-flow air was supplied to the nozzle which was generated through the glass beads and honeycomb. The high voltage was imposed on the central tube while the ground was set far away from the burner. Hence, the so-called single-electrode configuration was established. Figure 4(b) plots the schematic of a counter-flow burner which has an upper and a lower part. Each part features three co-axis annular slots. The central slot was designed for O_2 and fuel, while the inner and outer slots were used to stabilize the flame. The distance between the upper and the lower parts was adjustable according to the expected global parameters, e.g., strain rate. The upper part was grounded, while the positive terminal of the high-voltage power supply was connected to the lower part. Thus, an upward longitudinal electric field was established. This setup was first adopted by Tran et al. to measure the propagation of the edge flame [59,60]. Figure 4(c)

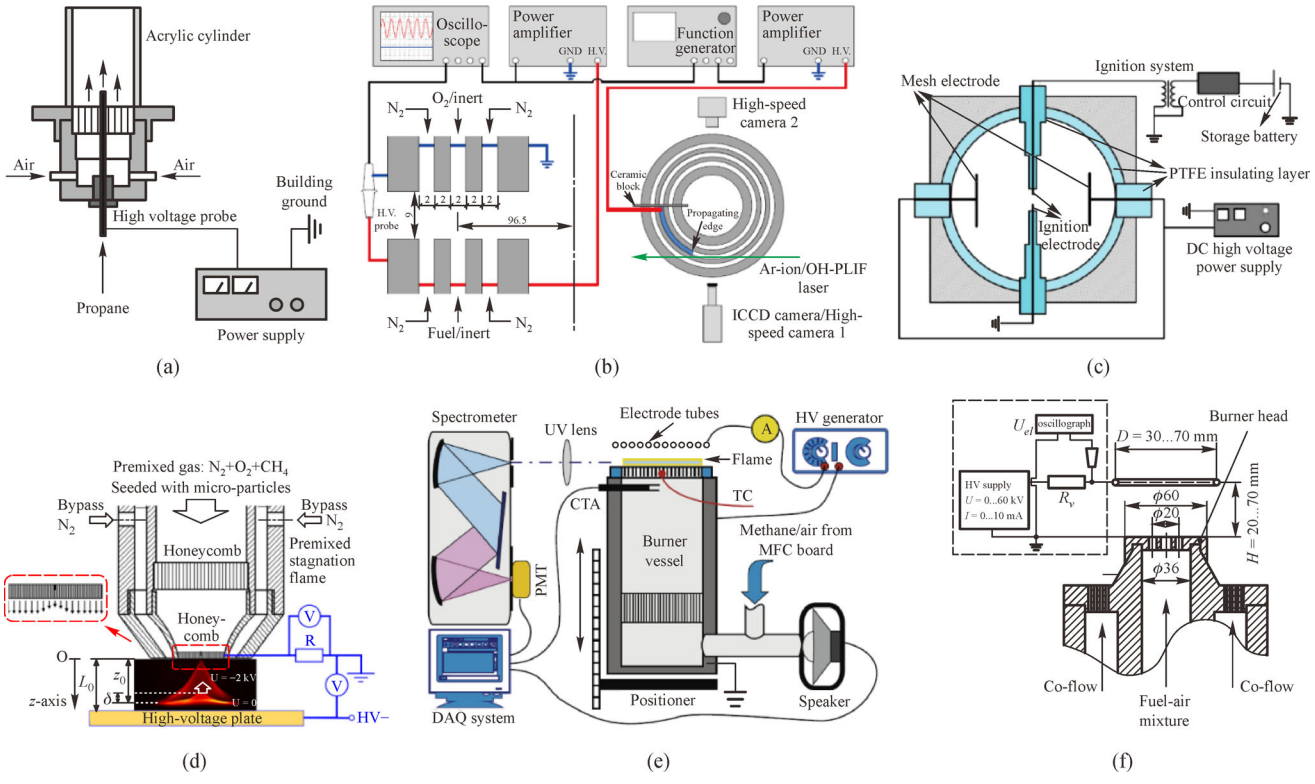

Fig. 4 Schematics of the experimental setup for EFAC system (adapted with permission respectively from Refs. [7,9,50,60,62,64]. (a) Co-flow jet flame buner; (b) counterflow flame buner; (c) constant-volume combustion bomb; (d) stagnation flame burner; (e) flat flame burner; (f) modular burner.

illustrates a constant-volume combustion bomb used to generate a spherically expanding flame that features a simple flame structure [23,61,62]. Typically, the bomb is cylindrical and the diameter equals the length. To impose an electric field on the flame, two electrodes were insulated by a polytetrafluoroethylene layer and connected to the output terminal of the DC/AC high-voltage power supply. The electrodes can be mesh-shaped as shown in Figure 4(c) or any other desired shapes. The ignition electrodes were vertically inserted into the bomb, which were also embedded within the polytetrafluoroethylene insulating layer. Since the flame spread in all directions, the phenomenon caused by transverse and longitudinal electric fields can be observed at the same time. Such a setup is suitable to study EFAC at different pressures. Figure 4(d) is the schematic of the stagnation flame burner. The premixed gas passed through the honeycombs and flowed into the nozzle. The bypass N_2 was added to protect the premixed gas from the turbulence of the environment. A stagnation plate was placed downstream and worked as the high-voltage terminal, while the burner was grounded. Such a burner can be used to observe the transition between the flat and conic flames under the effect of the electric field. Figure 4(e) exhibits the schematic of the flat flame burner [64], which consisted of a cylindrical vessel and a porous-plate. The premixed mixture was fed into the cylindrical vessel and then flowed through the porous-plate. Finally, the flat flame was stabilized near the surface of the burner. In this case, the electrode was made of thin stainless steel tubes and positioned above the burner. The high voltage was applied between the electrode and the burner. A loudspeaker was installed to generate acoustic oscillations. Therefore, this burner was suitable for the evaluation of the electric field effect on the thermo-acoustic response. Figure 4(f) illustrates a modular burner [7]. The premixed mixture was fed into the central channel while the co-flow was fed into the outer channel. The major advantage of this burner is the modular design. By changing the burner bead, different flame types can be produced. Up to now, three types have been tested based on this burner, i.e., 7-hole Bunsen flames, wire-stabilized V-flames as well as aerodynamically swirl-stabilized flames. Unfortunately, more details about the burner bead were not reported. A ring-shaped electrode was positioned above the burner and served as the high-voltage terminal while the burner was grounded. Based on this burner, the emission reduction was reported.

Apart from the focuses on the various flames and electric fields discussed above, numerous diagnostic techniques have been developed and adopted to measure different physical quantities of the EFAC as well, e.g., thermocouple for temperature, hot-wire for velocity, microphone for acoustic pressure, and so on. However, the aforementioned methods are all intrusive, which can disturb the flame and are insufficient to capture the true properties of the flames. Thus, optical diagnostics, which have the advantages of non-intrusiveness, have been developed. The cathetometer was adopted to measure the flame height [66]. Direct photography of the flame chemiluminescence by the camera or photomultiplier is a well-established optical diagnostic tool to analyze the flame response and stabilization. The images of the flame can be further analyzed to extract the temperature information by two-color pyrometry [67]. The flame temperature can be measured by infrared thermal distribution imaging as well [68]. The Schlieren method and shadow imaging are usually applied to visualize the flow of the flame and determine the flame front [55,62]. Recently, due to the rapid development of the laser technology, laser-based diagnostics have been widely adopted in the research of the EFAC. By illuminating the flame via a pulsed or continuous laser, various physical quantities can be captured and extracted. Among the advanced techniques, planar laser-induced fluorescence (PLIF) [26,69] based on the measurement of fluorescent signals of various radicals is the most popular technique. PLIF can capture two-dimensional distributions of radicals, e.g., CH*, OH*, and CHO*. Further processing the PLIF images, various flame properties, e.g., heat release rate and flame front, can be extracted. Apart from PLIF, there are other well-established laser-based techniques, for instance, particle image velocimetry (PIV) [70] to measure the flow velocity which is always conducted together with PLIF; Mie scattering to visualize the flow structure [71]; laser-induced incandescence [72] and laser extinction [15] to estimate the relative and absolute soot volume fraction, respectively; coherent anti-Stokes Raman scattering [35] for accurate temperature measurement. Benefited from the advances of the computer technology, tomography has been another promising technology that was first introduced for the diagnosis of EFAC in 2012 by Tretyakov et al. [73]. Compared with planar techniques, tomography can extract more useful information from a limited number of projections. In the experiment conducted by Tretyakov et al., the two-dimensional distribution of the CH* signal was reconstructed via the maximum entropy method based on the axisymmetric assumption. Ren et al. [57] applied Abel transform to extract the flame front. Later on, Park et al. [74] applied the three-dimensional method, i.e., the tomographic Mie scattering imaging to extract the bi-directional ionic wind. Besides the common quantities as measured in traditional combustion research, the electric characteristics are the special quantities in the EFAC. Typically, the voltage and the current can be monitored by the high-voltage probes and an oscilloscope [31,55]. The sub-breakdown electric field strength can be monitored by using the so-called electric-field-induced second harmonic generation method, which was introduced and successfully applied to the premixed stagnation flame by Ren et al. in 2020 [58]. This method was further improved by Butterworth and Cha [75], which requires no information of gas composition and temperature.

5 Emission reduction

It is well-recognized that combustion can generate various pollutants, including soot, CO, CO_2, and NO_x. Such pollutants will lead to global warming, acid rain, and other severe problems. To overcome such problems, numerous advanced combustion techniques and combustion systems have been developed to control and reduce pollutants. Among the techniques, EFAC is a promising one and has the advantage of low power consumption and fast response. It has been reported that positive ions could serve as the nuclei of soot particles but not the negative ions [67]. Therefore, most soot particles carry positive charges and will move to the negative electrode due to the Lorentz force [72]. Figure 5 is a comparison of thermophoretic sampling particle diagnostics (TSPD) images at different polarity and strength of the electric field at various heights above burner (HAB). Two magnifications are selected for better display at 2 μm and 300 mm, respectively. The TSPD images at a lower HAB indicate the primary size of the soot particles, while the images at a higher HAB capture the agglomerate size. As can be seen, the primary particle size is not dependent on the electric field but the agglomerate is [72]. Laser-induced incandescence [76] and laser extinction [15] have verified that the directional movement of the soot can change the resistance time and then change the soot volume fraction in the flame. The initial rate of deposition on the electrode can be altered as well. Such a property has been used to extract the soot from the flames [77]. The research has shown that the electric field also considerably influences the formation and growth of the soot by intensifying the oxidation. The reduction of soot in the flame depends on the polarity and strength of the electric field. The efficiency of soot suppression is around 90% (70%) under the upward (downward) longitudinal electric field [67]. However, there is a voltage range where the quantity of soot can be larger than that without the electric field due to the competition between the soot formation and soot removal [78]. Apart from soot, the electric field can increase the yield of fullerenes and decrease the yield of polycyclic aromatic hydrocarbons in benzene flames [78].

As to the NO_x emission, a reduction is observed on the flame channel flows embedded in a radial transverse DC electric field, which can be attributed to the enhancement of the heat transfer to the walls [79,80]. Similar to the soot, the polarity of the electric field affects the generation of CO and NO_x, irrespective of pressure. The concentration of CO was reduced by 90% accompanied by the slight increase of NO_x under the downward longitudinal electric field while the opposite phenomenon was observed under the reversed electric field [31]. The reduction of the CO was also predicted by the two-dimensional simulation based on computational fluid dynamics [81]. Figure 6 plots the pollutant emission, i.e., unburnt hydrocarbon (UHC), CO, NO_x as well as flame cone angle as a function of reduced voltage (voltage divided by pressure). As can be seen, the UHC has a similar behavior to CO, while the angle holds the opposite trend [7]. The different behavior of CO and NO_x can be attributed to the change of the gap, where incomplete combustion exists between the reaction zone and the burner rim under the electric field. The reduction of the gap leads to a more complete combustion and a rise of temperature, which have been verified by coherent-anti-Stokes Raman spectroscopy. The ionic wind can reduce the flow velocity, which increases the residual time and

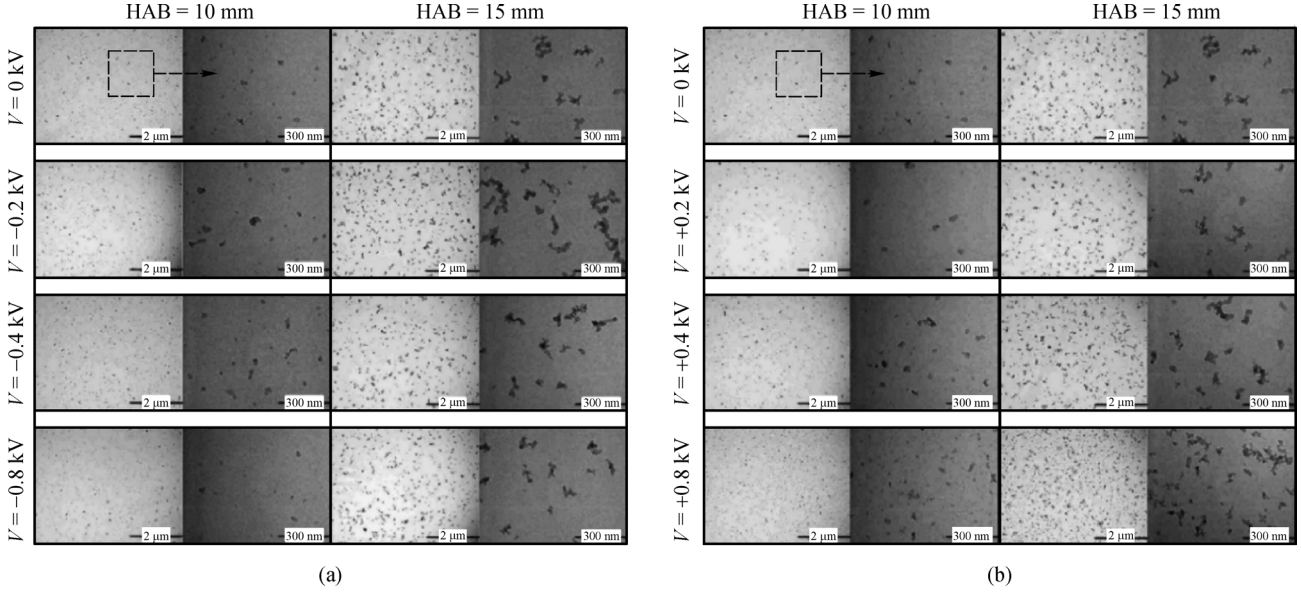

Fig. 5 TSPD images at HAB = 10 mm and 15 mm.
(a) Without/with upward field; (b) without/with downward field (adapted with permission from Ref. [72]).

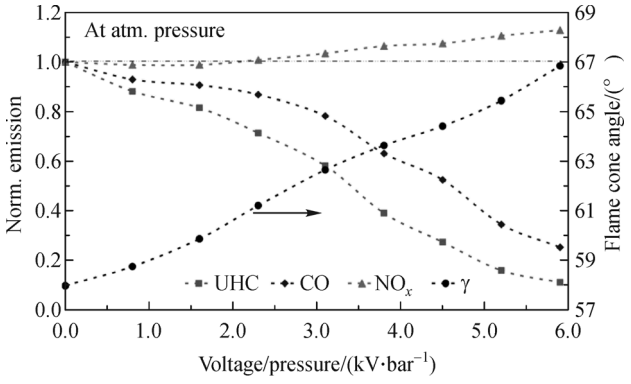

Fig. 6 Pollutant emission and flame cone angle as a function of reduced voltage (adapted with permission from Ref. [7]).

temperature as well. As a consequence, the CO decreases while NO_x increases [82]. On the other hand, the electric field can improve the lean blow-off limit and reduce the generation of NO_x at a low equivalence ratio [7,83]. A reduction of about 40% of NO_x was reported under the electric field with proper electrodes [83]. By keeping the flame undistorted, the marginal effects of the electric field on the NO was observed, while CO, CO_2 were reduced due to the directional movement of the charged soot particles. The impacts on the CO, CO_2, and NO vanished with the increase of O_2 [84]. Different from the DC electric field, three voltage regimes of longitudinal HF electric field (10 kHz) can be found. In the low (<1 kV) and high (>3 kV) voltage regimes, the CO molar fraction increases while the NO molar fraction decreases. However, in the intermediate (1–3 kV) voltage regime, an opposite phenomenon was observed [85]. For readers' convenience, Table 1 summarizes the impact of the electric field on flame emission.

6 Flame stabilization

Flame stabilization is another hot topic of EFAC. The electric field can either stabilize the flame or cause instability accompanied by the alternation of the flame shape, flame luminosity, and acoustic oscillation. Of the various phenomena of instability, the change of the flame shape is the most evident observation, which is induced by the transverse DC electric field and was first observed by Brande [6]. It has been reported that the longitudinal DC electric field can decrease the height of the flames, irrespective of the polarity in most cases [78]. The reduction of the flame height, as well as the increase of the flame width, is more evident under the downward electric field [15,43]. If the applied voltage increases up to the threshold, the flame shape begins to be deformed, oscillated, and collapsed, especially under an upward electric field [15,35]. In such a case, the increase of the average flame height is also possible [16]. Further increasing the voltage, different instabilities occurred. The oscillation of the flame under a DC electric field can be attributed to the competition between upward ionic wind and the premixing at the burner rim [45]. If the voltage is high enough, the hissing sound occurs due to the corona discharge. The deformation of the flame shape is more sensitive to the upward electric field. For example, a spreading phenomenon of the flame tip can be observed which does not occur under a downward DC electric field [67]. As for HF electric field, the yellowish zone is narrower in the low voltage regime, becomes larger in the intermediate voltage regime, and disappears in the high voltage regime accompanied by the hissing noise [85].

For different flow and electric field parameters, various oscillation modes have been found under electric fields. A

Table 1 Relationship between emission and electric field

Properties	Flame type	AC	Downward DC	Upward DC	Transverse DC
NO_x emission	Premixed turbulent/laminar jet flame (methane) [31,84]	–	Minimal	Minimal	–
	Non-premixed laminar jet flame (methane) [85]	<1 kV: decrease 1 kV–3 kV: increase >3 kV: decrease	–	–	–
	Premixed flame channel flows (propane) [80]	–	–	–	Decrease
CO emission	Premixed turbulent/laminar jet flame (methane) [31,84]	–	Decrease	Increase	–
	Non-premixed laminar jet flame (methane) [85]	<1 kV: increase 1 kV–3 kV: decrease >3 kV: increase	–	–	–
UHC emission	Premixed swirl-stabilized (fuel not reported) [7]	–	Decrease	–	–
Soot	Non-premixed jet flame (acetylene and ethylene) [15,67]	–	Decrease	Decrease	–
	Non-premixed counterflow flame (ethylene) [76]	–	Decrease	–	–

series of images of a jet flame without and with imposed downward DC electric field are presented in Fig. 7. The time interval between the three successive images under the electric field is 38 ms. As can be seen, the oscillation of the flame height at 3 kV downward DC electric field is obvious, which is alternatively longer and shorter than that without electric field. Based on the observation of the flame height, the oscillation frequency can be extracted by fast Fourier transform. Figure 8 plots the four oscillation modes under an AC electric field based on the time evolution of the edge height of the lifted flame. The flowrate, voltage, and frequency are labeled as well. Mode A features random fluctuation and no specific frequency can be extracted. Mode B has a large oscillation around the flame frequency. Mode C has a small oscillation embedded within a large oscillation. Mode D has a small oscillation synchronized to the AC frequency [36]. Both Modes C and D feature the frequency-doubling behavior, which can be attributed to the buoyancy effect [86]. A contrary behavior, named period-doubling behavior, i.e., the co-existence of the synchronized frequency and its half frequency, is also observed on the premixed edge flame. Other modes are also identified according to the modified flame shape. In the negative voltage half period of the AC electric field, the negatively charged burner can generate O_2^-, which is forced by the upward Lorentz force. However, in the next positive voltage half period, the negatively charged particles are pulled by the burner rim. The fluctuating force can trigger instability and lead to a branch of the flow [71]. Apart from the direct photography of the flame, planar laser-induced fluorescence (PLIF) captures the more detailed structure of the flame. The results of CHO PLIF show that the flame front is stretched under the electric field, while OH PLIF indicates that the reaction zone is broadened [70]. The width of the reaction zone is observed to have increased by 380% via the combination of the OH/acetone PLIF when the flame becomes unstable [26]. From another point, a hypothesis regarding the electromagnetic effect of the AC electric field was proposed, i.e., the AC electric field can induce the magnetic field and form the toroidal vortex within the jet diffusion flame [8,87]. In such a case, the charged particles are subjected to electromagnetic fields at the same time. When frequency and voltage are beyond a critical value, i.e., $fU^2 = 2.7\times 10^9$ Hz·V^2, the magnetic field can trigger the generation of the inner toroidal vortex and the ionic wind can magnify this influence. The existence of the inner toroidal vortex can deposit the soot and further induce the generation of the outer toroidal vortex. The two toroidal vortexes can result in flame instability, e.g., spinning and pinch-off modes.

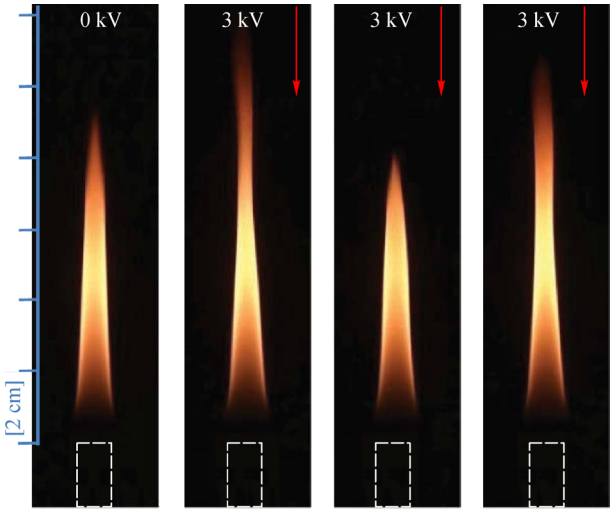

Fig. 7 Images of a jet flame without and with downward DC electric field at the time interval between the three successive images under the electric field of 38 ms (adapted with permission from Ref. [15]).

When considering the counterflow flame, two different oscillation modes are observed on the balanced position of the flame, i.e., constant oscillation amplitude in the low frequency (less than 20 Hz) regime and quickly decaying amplitude in high-frequency regime [54]. Moreover, it has been reported that the electric field can either suppress or induce acoustic oscillation through unsteady combustion [34,57,88]. By imposing a DC electric field on the spherically expanding flame, the flame becomes ellipsoidal due to the different flame propagation along the vertical and horizontal directions [23,61]. The spherically expanding flame is cracked under the HF electric field, which can be attributed to electro-hydrodynamic instability and thermo-diffusive instability [89]. Recently, a theoretical mechanism was proposed by Ren et al. to explain the electro-hydrodynamic instability [50]. They reported that the wrinkled flame surface under the DC electric field can increase the electric body force, which can further deform the flame shape. Such positive feedback eventually induces flame instability. Besides, more deficient light radicals, e.g., O, H, and OH are generated under the electric field. These radicals have high mass diffusivities, resulting in a Lewis number of the flame below unity. Hence, thermo-diffusive instability occurs [51].

The flow characteristics of jet flames have also been extensively investigated by Cha and coworkers with the single-electrode configuration [55,56,66]. They reported that the DC electric field had little impact on the liftoff height and reattachment velocity. The liftoff property is reproduced by a simple simulation model, where a detailed mechanism for neutral particles and simplified mechanisms for ions are adopted [90]. However, the positive DC electric field can decrease the blow-off velocity, while the negative electric field holds the opposite impact [38]. The HF electric field can convert the liftoff flame into an attached flame, increase the blow-off velocity, and further

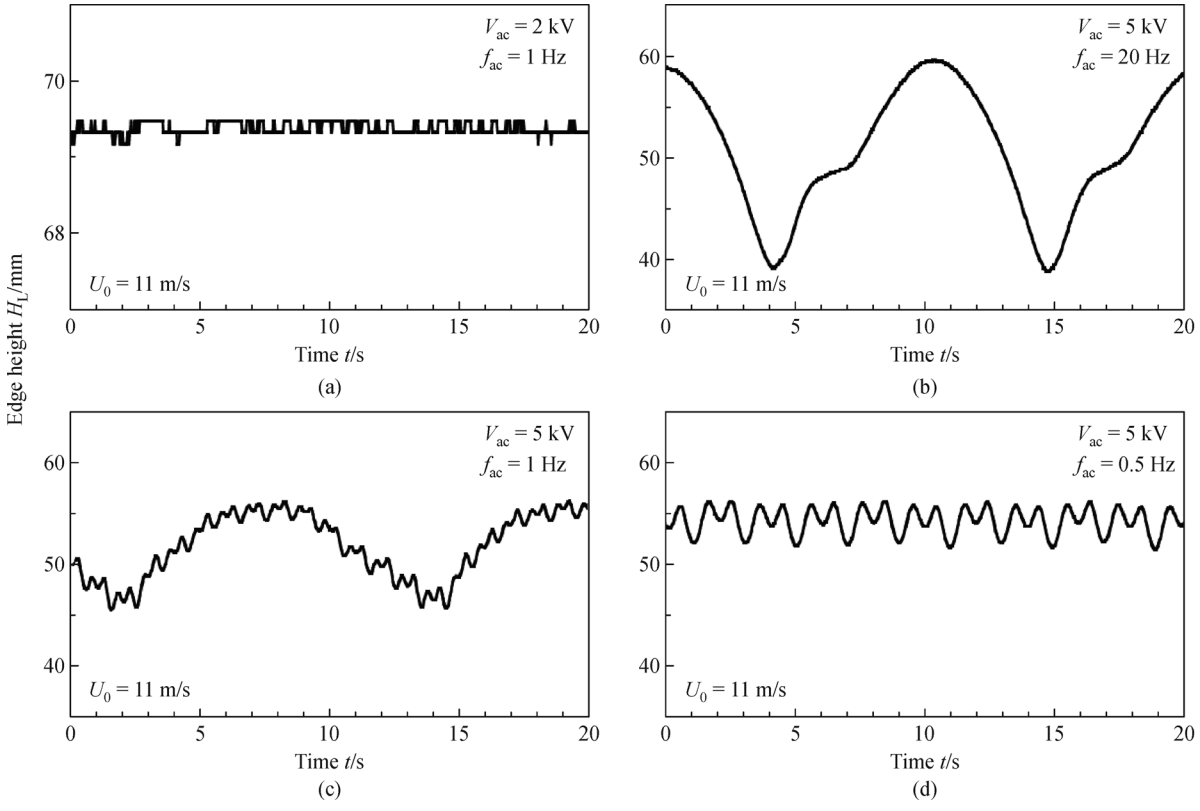

Fig. 8 Height oscillation modes under low-frequency AC electric field (adapted with permission from Ref. [36]). (a) Mode A; (b) mode B; (c) mode C; (d) mode D.

improve flame stability. Under the low-frequency AC electric field, the blow-off velocity is reduced, which can be attributed to the bi-directional ionic wind [38]. If combining blow-off velocity and liftoff velocity, the so-called detachment velocity is proposed, and different correction functions are defined to express the relationship between the detachment velocity, AC voltage, and frequency [66]. In the low voltage regime (less than 4 kV), the detachment velocity increases with the AC voltage and frequency. In the intermediate voltage regime (between 4 kV and 6 kV), the detachment velocity decreases with the AC voltage and is independent of the frequency. In the high voltage regime (larger than 6 kV), a weak dependence on AC voltage and frequency is reported [56]. The reattachment velocity increases with the increase of the applied voltage and decreases with the voltage frequency. Besides, the blowout velocity is not influenced by the AC electric field. The blow-off equivalence ratio of a jet flame is also reported to be slightly reduced under the longitudinal DC electric field [21]. The improvement is limited below 3% and increased with pressure [31]. However, no improvement of the blow-off limit is found on the swirl flame [7]. The relationship between the flow characteristics of flames and the electric field is summarized in Table 2.

7 Flame propagation

There are several well-established parameters about flame propagation, i.e., flame displacement speed, unburnt flow velocity, and flame speed/burning velocity. The flame speed can be obtained by the vector summation of the flame displacement speed and the unburnt gas velocity [9]. The flame propagation and speed modification of the EFAC have been extensively investigated by different research groups based on different flames. The team of Cha and Chung from King Abdullah University of Science and Technology [9,55,56,59,60,91] adopted jet and counter-flow flames in their experiments. It has been reported that the transverse and longitudinal electric fields have different impacts on flame propagation. Under the transverse AC/DC electric field, the flame displacement velocity is significantly reduced, while the flame propagation is almost unaffected, indicating no thermal or chemical effect [59,60]. However, under the longitudinal AC/DC electric field, the flame displacement velocity is enhanced and the velocity of the unburnt mixture is reduced. The propagation of the flame edge can be correlated with the flame curvature [91] and the increase of the propagation is also reported under the longitudinal AC/DC electric field [9]. More detailed measurements by PIV of a jet flame as

Table 2 Relationship between flow characteristics of flames and electric field

Properties	Flame type	AC voltage	AC frequency	DC voltage
Detachment velocity	Non-premixed laminar jet flame (propane) [56]	< 2–4 kV: linear increase	Increase ~$f^{0.38}$	Minimal
		(2–4)–5.5 kV: linear decrease	Minimal	Minimal
		> 5.5 kV: weak dependence	Weak dependence	Minimal
Liftoff velocity	Non-premixed turbulent jet flame (propane) [66]	Linear increase	Increase ~log(f/29.5)	Minimal
Blow-off velocity	Premixed laminar jet flame (methane) [38]	< 40 Hz: decrease	Decrease	Minimal
		40–50 Hz: minimal	Minimal	
		> 60 Hz: increase	Increase	
Reattachment velocity	Non-premixed laminar jet flame (propane) [55]	Linear increase	Decrease $1/f^{0.37}$	Minimal
Blow-off equivalence ratio	Premixed turbulent jet flame (methane) [31] Premixed bluff-body stabilized flame (propane) [21]	–	–	Decrease
	Premixed swirl-stabilized (fuel not reported) [7]	–	–	Minimal

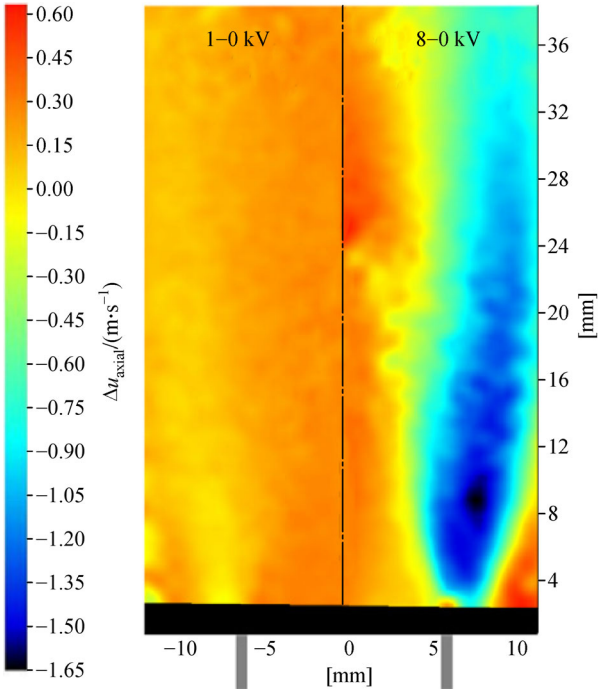

Fig. 9 Differential images of axial velocity for 1.0–0.0 kV and 8.0–0.0 kV (adapted with permission from Ref. [70]).

presented in Fig. 9 shows that the axial flow velocity in the central part of the flame is increased while that in the post-reaction zone is decreased [70]. The PIV measurements also confirm that the flame root is pushed to the burner room while the exhaust region is broadened [82]. The modification of the flow velocity is more evident for the rich mixture [37]. Such phenomena indicate that the electric field exerts influence on the flow velocity at first, which further modifies the flame, e.g., the relocation of the flame edge and modification of the flame shape [60]. Recently, the three-dimensional structure of the bi-directional ionic flow was qualitatively visualized by Park et al. [74]. From another point, the mass diffusivities of the ions in the reaction zone are increased by the electric field, which further decreases the Lewis number. As discussed in Section 6, the low Lewis number can induce thermos-diffusive instability, crack the flame, and enhance the burning velocity. Up to now, research has shown that the burning velocity can be enhanced by different degrees according to the flame type and the electric field, ranging from 2.5% to 200% [25,35,64]. The change of the burning velocity is also found to have an exponential relation with the applied voltage imposed on the flat flame [92].

Besides, the impacts of the electric field on the spherically expanding flames were studied by researchers from Xi'an Jiaotong University [23,61,93,94]. Three types of flame speed were defined, i.e., the vertical flame speed, the horizontal flame speed, and the average flame speed. The flame speed is derived from the visualization of the Schlieren method [23] by the assumption that no unburnt gas velocity exists. Figure 10 plots the typical flame propagation of the spherically expanding flames under DC electric fields. For these cases, the flames are generated within a constant volume combustion chamber, which is similar to the setup shown in Fig. 4(c). Two mesh electrodes are inserted into the chamber horizontally and connected to the high-voltage terminal of the high-voltage power supply. In Fig. 10, the flame deformation is observed as well. It was reported that the average flame speed increased linearly with the applied voltage under the DC electric field and was more pronounced for lean mixture [23,62]. Moreover, the uniformity of the electric field strength played a significant role in the flame speed, i.e., the larger uniformity could better enhance the flame speed. Under a low-pressure condition, the horizontal electric field could suppress the vertical flame speed. However, the vertical flame speed was found to be enhanced under a high-pressure condition. Such a transition could be attributed to the occurrence of the flame instability induced by the high pressure [94]. In the

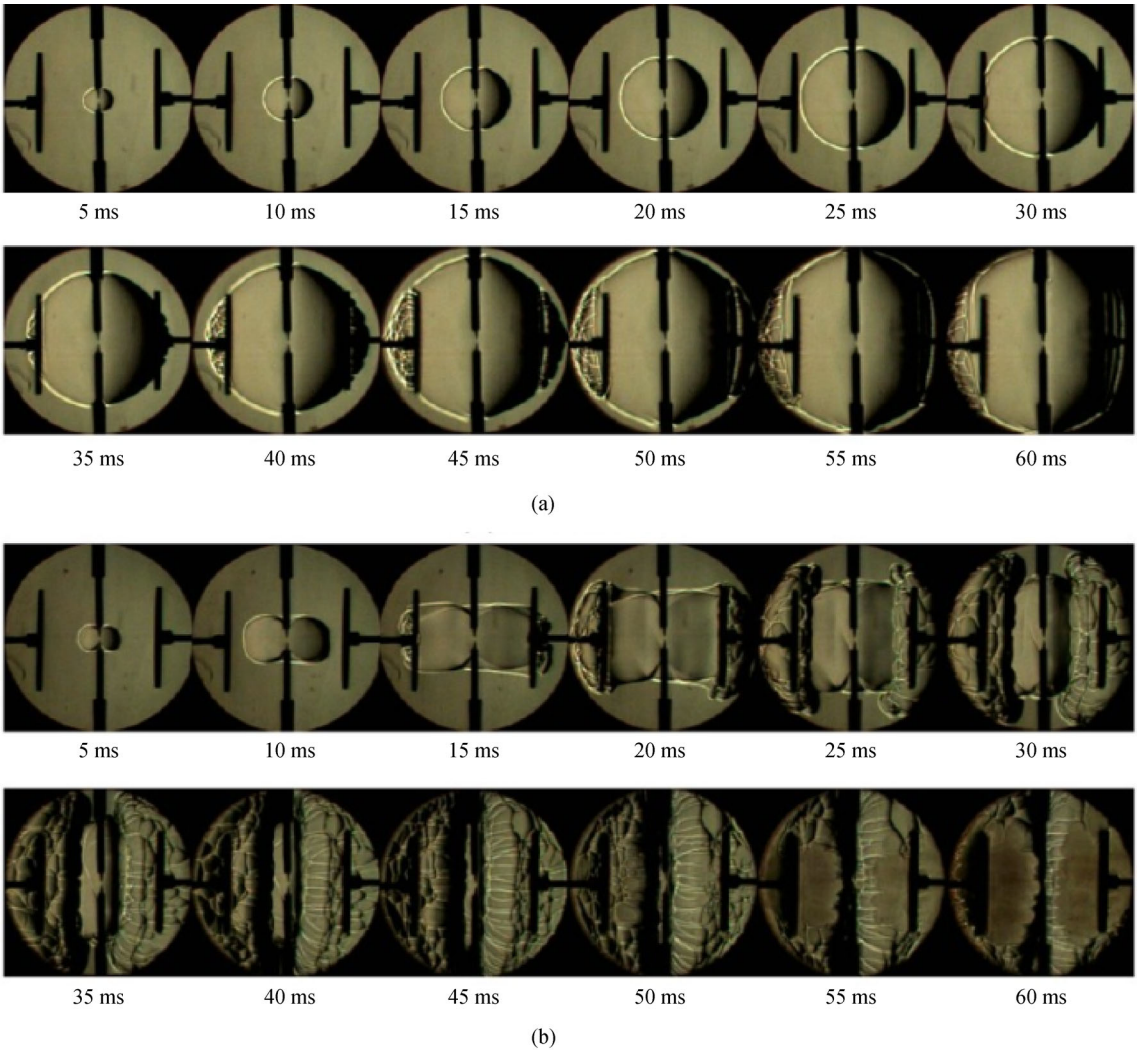

Fig. 10 Flame propagation of spherically expanding flames under DC electric field (adapted with permission from Ref. [62]). (a) $U = 0$ kV; (b) $U = -15$ kV.

spherically expanding flame, various flow was found as shown in Fig. 11. Two vortexes (in blue arrows) were found on both sides of the flame surface and were induced by the movement of the flame surface due to the existence of viscosity which could further change the flow field [95]. The red arrows represent the movement of the flame surface, while the big green arrow and purple arrows indicate the inner and outer flow, respectively. During the propagation, a sudden acceleration stage was found, which could be explained by the positive feedback loop between the electric body force and the crack of the flame [94]. The HF electric field had a different impact on the propagation of the spherically expanding flame. The average flame speed had a positive correlation with the voltage frequency and an exponential correlation with the applied voltage. However, when the frequency was beyond 25 kHz, the average velocity reached its maximum and kept a stable value. Under the HF electric field, the response time (approximately 10 ms) of the ionic wind was far larger than the period (less than 1 ms) of the electric field. Therefore, the impact was mainly attributed to the direct chemical effect of the electric field and the trigger of flame instability [61,89]. For hydrogen enhancement combustion, it was found that the flame speed could be accelerated and the electric field effect could be suppressed [93]. However, a detailed analysis is still unknown. For readers' better understanding, Table 3 summarized the impact of electric field on flame propagation.

8 Concluding remarks and future work

To sum up, this paper reviews the recent progress of electric-field assisted combustion which is a complicated coupling system of chemistry, physics, and electromagnetics and provides significant opportunities and chal-

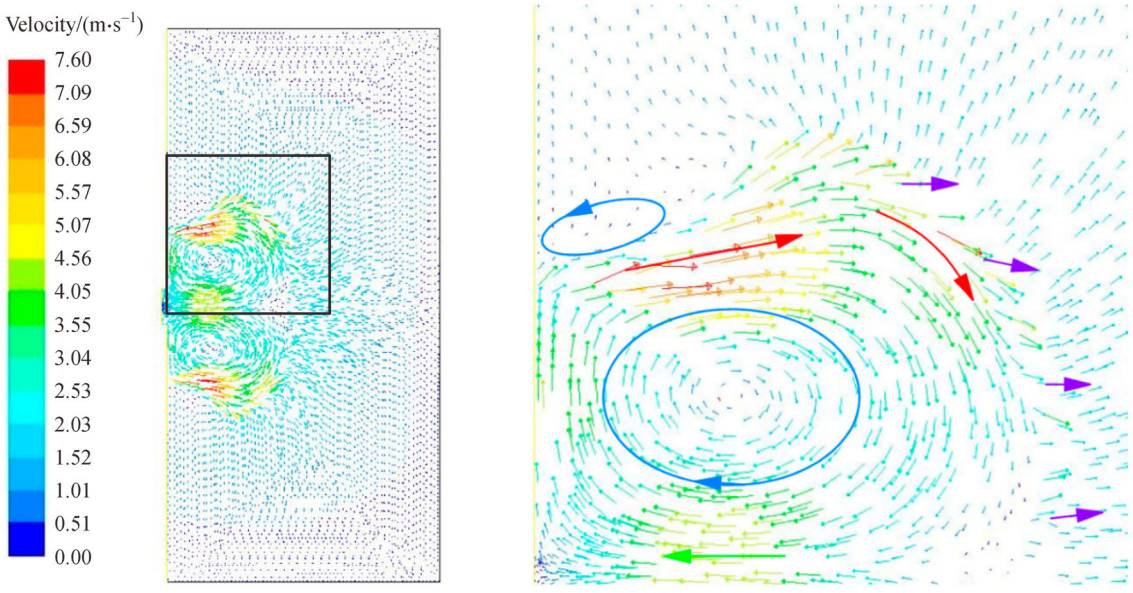

Fig. 11 Right side of flow velocity for spherically expanding flame at a voltage of 5 kV after 34 ms (adapted with permission from Ref. [95]).

Table 3 Relationship between flame propagation and electric field

Properties	Flame type	Longitudinal AC voltage	Longitudinal DC voltage	Transverse AC voltage	Transverse DC voltage
Flame speed	Premixed jet flame (propane) [35]	–	Increase	–	–
	Premixed flat flame (methane) [92]				
	Premixed spherical flame (methane and propane) [23,61,62,89,94]	Increase	Increase	–	Increase (0.1–0.3 MPa); decrease (0.5 MPa)
Flame displacement velocity	Non-premixed laminar lifted flame (propane) [91]	Increase	Increase	–	–
	Non-premixed counterflow flame (methane and propane) [59,60]	–	–	Decrease	Decrease
Unburned velocity	Non-premixed laminar lifted flame (propane) [91]	Decrease	Decrease	–	–
Propagation speed	Non-premixed laminar jet flame [9]	Increase	Increase	–	–
	Non-premixed counterflow flame (methane and propane) [59,60]	–	–	Minimal	Minimal

lenges for the control of the combustion phenomena. Up to now, extensive research effort has been devoted to investigating the basic impacts of the alternating/direct current electric field on various kinds of flames. Three mechanisms, i.e., the ionic wind effect, the chemical effect, and the Joule heat effect, have been proposed to explain the electric-field-induced phenomena. Besides, a non-monotonic phenomenon between alternating current electric field frequency and blow-off velocity is observed and can be attributed to the so-called bi-ionic wind effect. To better understand the bi-ionic wind effect, a parameter called the developing degree of the ionic wind has been proposed. Various experiment setups have been designed and applied, including the jet burner, the counterflow burner, the constant-volume combustion bomb, the stagnation burner, and so on. The optical and non-optical diagnostics have been introduced in the experiments. There are three typical regimes for the voltage-current characteristics, i.e., the sub-saturation regime, the saturation regime, and the super-saturation regime. However, the more complicated voltage-current characteristics have been observed as well. Moreover, the reduction of the CO and unburnt hydrocarbon accompanied by the increase of the NO_x has been reported under the downward longitudinal direct current electric field, while the opposite phenomena has been detected under the reverse electric field. The generation of

the soot is also dependent on the polarity and electric field strength. The electric field can either induce flame instability or stabilize the combustion. The instabilities, including electro-hydrodynamic instability and thermos-diffusive instability, are reported. Various instability modes are induced, i.e., the oscillation mode, the spinning mode, the branch-off mode, and the pitch-off mode. As to the flame propagation, it is reported that the electric field has no impact on the flame propagation, but merely modifies the flow velocity. On the contrary, the enhancement of the flame speed is observed on the spherically expanding flame.

The above findings create many opportunities in the scientific research and development of electric-field assisted combustion. Similar to plasma-assisted combustion, electric-field assisted has a great potential for applications in gas turbines and internal combustion engines [14]. For example, it can extend the lean blow-off limit, stabilize the combustion, and further decrease the pollutant emission which are the requirements of an advanced combustion system. The closest example to practical application is the investigation within the constant volume bomb, where the electrodes are inserted into the bomb through the wall. The schematic is similar to Fig. 4(c). The flame speed, pressure, temperature, and combustion duration time have been extensively tested under different pressure and electric field, which has laid the foundation for practical applications. By imposing a high-voltage electric field on the combustor, it is necessary to add the insulating material. However, it is still a problem to choose a proper insulating material which has qualified mechanical and thermal properties. Besides, the mechanical integration of the high voltage power supply system and the combustor is an open question, which is related to the mechanical stabilization of the system. In addition, the existing mechanisms have not been validated in practical combustors which may feature harsher conditions, e.g., high turbulence and high pressure. This should be the focus of future works.

In principle research, some contradictory results, e.g., different observations about flame propagation under different conditions have been reported indicating that there are large gaps in fundamental understanding, especially under complex combustion conditions. Therefore, in experimental studies, it is urgent to conduct the so-called fundamental experiments which have well-established conditions and easy to model by analytical and simulative approaches. Such experiments do not require simple conditions, but well-defined ones. Therefore, besides the simple flames, more complicated flames in practical engines are also required, e.g., multi-nozzle swirl-stabilized flames. The understanding of the coupling between physics, chemistry, and electromagnetics remains challenging and the chemical reaction pathway is still unclear. When other particles (NaOH, H_2, and so on) are added which are commonly used in combustion systems, the coupling relationship becomes even more difficult to understand. Moreover, there is no systematic research about flame propagation numbers, i.e., Markenstein, stretch factors, etc. under the electric field, which should be the focus in the future as well.

There are still limited research on modeling and simulation. Accurate simulation of the electric-field assisted combustion is still difficult due to the various temporal and spatial scales. One of the major difficulties to simulate electric-field assisted combustion is to gain the microscopic properties of the ions, like the collision cross-section, potential model, and so on. The ion chemistry is one of the key problems in the simulation as well. Besides, the lack of quantitative results and clear boundary conditions of the experiments also restricts the development of the simulation. The experimental data and the theoretical calculation need to be further cross-validated. To extract more spatiotemporal information, the traditional methods, e.g., thermocouples and hotwires, cannot satisfy such requirements anymore and the multi-physical multi-dimensional measurements are the trends of development. Such measurements require more advanced diagnostics, e.g., tomographic particle image velocimetry [96], tomographic laser-induced incandescence [97], volumetric laser-induced fluorescence [98], and background-oriented Schlieren tomography [99]. Moreover, the electric parameters should be measured as well, e.g., electron density. To address these challenges, more efforts on the test rigs, diagnostics, and simulation are required.

Acknowledgements This work was funded by National Natural Science Foundation of China (Grant No. 51976122), the Foundation of Science and Technology on Combustion and Explosion Laboratory (Grant No. 6142603200508), and the National Science and Technology Major Project 2017-III-0007-0033.

References

1. Chefurka P. World energy and population. 2007, available at the website of paulchefurka.ca
2. Cai W, Kaminski C F. Tomographic absorption spectroscopy for the study of gas dynamics and reactive flows. Progress in Energy and Combustion Science, 2017, 59: 1–31
3. Lu X, Han D, Huang Z. Fuel design and management for the control of advanced compression-ignition combustion modes. Progress in Energy and Combustion Science, 2011, 37(6): 741–783
4. Benard P, Lartigue G, Moureau V, et al. Large-eddy simulation of the lean-premixed preccinsta burner with wall heat loss. Proceedings of the Combustion Institute, 2019, 37(4): 5233–5243
5. Wang Y, Le J. A hollow combustor that intensifies rotating detonation. Aerospace Science and Technology, 2019, 85: 113–124
6. Brande W T. The bakerian lecture: on some new electro-chemical phenomena. Philosophical Transactions of the Royal Society of London, 1814, 104: 51–61
7. Altendorfner F, Beyrau F, Leipertz A, et al. Technical feasibility of electric field control for turbulent premixed flames. Chemical

Engineering & Technology, 2010, 33(4): 647–653
8. Xiong Y, Chung S H, Cha M S. Instability and electrical response of small laminar coflow diffusion flames under AC electric fields: toroidal vortex formation and oscillating and spinning flames. Proceedings of the Combustion Institute, 2017, 36(1): 1621–1628
9. Won S H, Ryu S K, Kim M K, et al. Effect of electric fields on the propagation speed of tribrachial flames in coflow jets. Combustion and Flame, 2008, 152(4): 496–506
10. Liu H, Sun B, Cai W. kHz-rate volumetric flame imaging using a single camera. Optics Communications, 2019, 437: 33–43
11. Tang Y, Zhuo J, Cui W, et al. Non-premixed flame dynamics excited by flow fluctuations generated from dielectric-barrier-discharge plasma. Combustion and Flame, 2019, 204: 58–67
12. Barkley S J, Zhu K, Lynch J E, et al. Microwave plasma enhancement of multiphase flames: on-demand control of solid propellant burning rate. Combustion and Flame, 2019, 199: 14–23
13. Zhang Y, Li S, Ren Y, et al. Two-dimensional imaging of gas-to-particle transition in flames by laser-induced nanoplasmas. Applied Physics Letters, 2014, 104(2): 023115
14. Ju Y, Sun W. Plasma assisted combustion: dynamics and chemistry. Progress in Energy and Combustion Science, 2015, 48: 21–83
15. Gillon P, Gilard V, Idir M, et al. Electric field influence on the stability and the soot particles emission of a laminar diffusion flame. Combustion Science and Technology, 2019, 191(2): 325–338
16. Liu H, Yang Z, Cai W. Application of three-dimensional diagnostics on the direct-current electric-field assisted combustion. Aerospace Science and Technology, 2021, 112: 106657
17. Bradley D, Nasser S H. Electrical coronas and burner flame stability. Combustion and Flame, 1984, 55(1): 53–58
18. Lawton J, Weinberg F. Electrical Aspects of Combustion. Oxford: Clarendon Press, 1969
19. Yagodnikov D A, Voronetskii A V. Effect of an external electrical field on ignition and combustion processes. Combustion, Explosion, and Shock Waves, 1994, 30(3): 261–268
20. Fialkov A B. Investigations on ions in flames. Progress in Energy and Combustion Science, 1997, 23(5–6): 399–528
21. Ata A, Cowart J S, Vranos A, et al. Effects of direct current electric field on the blowoff characteristics of bluff-body stabilized conical premixed flames. Combustion Science and Technology, 2005, 177 (7): 1291–1304
22. Calcote H F. Ion production and recombination in flames. Symposium (International) on Combustion, 1961, 8(1): 184–199
23. Duan H, Wu X, Sun T, et al. Effects of electric field intensity and distribution on flame propagation speed of $CH_4/O_2/N_2$ flames. Fuel, 2015, 158: 807–815
24. Park D G, Chung S H, Cha M S. Bidirectional ionic wind in nonpremixed counterflow flames with DC electric fields. Combustion and Flame, 2016, 168: 138–146
25. Garanin A F, Tret'yakov P K, Tupikin A V. Effect of constant and pulsed-periodic electric fields on combustion of a propane-air mixture. Combustion, Explosion, and Shock Waves, 2008, 44(1): 18–21
26. Schmidt J, Ganguly B. Effect of pulsed, sub-breakdown applied electric field on propane/air flame through simultaneous OH/acetone PLIF. Combustion and Flame, 2013, 160(12): 2820–2826
27. Wilson H A. Electrical conductivity of flames. Reviews of Modern Physics, 1931, 3(1): 156–189
28. Carleton F B, Weinberg F J. Electric field-induced flame convection in the absence of gravity. Nature, 1987, 330(6149): 635–636
29. Hu J, Rivin B, Sher E. The effect of an electric field on the shape of co-flowing and candle-type methane-air flames. Experimental Thermal and Fluid Science, 2000, 21(1–3): 124–133
30. Bisetti F, El Morsli M. Calculation and analysis of the mobility and diffusion coefficient of thermal electrons in methane/air premixed flames. Combustion and Flame, 2012, 159(12): 3518–3521
31. Sakhrieh A, Lins G, Dinkelacker F, et al. The influence of pressure on the control of premixed turbulent flames using an electric field. Combustion and Flame, 2005, 143(3): 313–322
32. Lawton J, Mayo P J, Weinberg F J. Electrical control of gas flows in combustion processes. Proceedings of the Royal Society of London. Series A, Mathematical and Physical Sciences, 1968, 303(1474): 275–298
33. Kono M, Carleton F B, Jones A R, et al. The effect of nonsteady electric fields on sooting flames. Combustion and Flame, 1989, 78 (3–4): 357–364
34. Kuhl J, Jovicic G, Zigan L, et al. Influence of electric fields on premixed laminar flames: visualization of perturbations and potential for suppression of thermoacoustic oscillations. Proceedings of the Combustion Institute, 2015, 35(3): 3521–3528
35. Marcum S D, Ganguly B N. Electric-field-induced flame speed modification. Combustion and Flame, 2005, 143(1–2): 27–36
36. Ryu S K, Kim Y K, Kim M K, et al. Observation of multi-scale oscillation of laminar lifted flames with low-frequency AC electric fields. Combustion and Flame, 2010, 157(1): 25–32
37. Kuhl J, Jovicic G, Zigan L, et al. Transient electric field response of laminar premixed flames. Proceedings of the Combustion Institute, 2013, 34(2): 3303–3310
38. Kim M K, Chung S H, Kim H H. Effect of electric fields on the stabilization of premixed laminar Bunsen flames at low AC frequency: bi-ionic wind effect. Combustion and Flame, 2012, 159(3): 1151–1159
39. Belhi M, Domingo P, Vervisch P. Modelling of the effect of DC and AC electric fields on the stability of a lifted diffusion methane/air flame. Combustion Theory and Modelling, 2013, 17(4): 749–787
40. Belhi M, Lee B J, Cha M S, et al. Three-dimensional simulation of ionic wind in a laminar premixed Bunsen flame subjected to a transverse DC electric field. Combustion and Flame, 2019, 202: 90–106
41. Chen Q, Yan L, Zhang H, et al. Electrical characteristics, electrode sheath and contamination layer behavior of a meso-scale premixed methane-air flame under AC/DC electric fields. Plasma Science & Technology, 2016, 18(5): 569–576
42. Borgatelli F, Dunn-Rankin D. Behavior of a small diffusion flame as an electrically active component in a high-voltage circuit. Combustion and Flame, 2012, 159(1): 210–220
43. Gan Y, Wang M, Luo Y, et al. Effects of direct-current electric fields on flame shape and combustion characteristics of ethanol in small scale. Advances in Mechanical Engineering, 2016, 8(1): 168781401562484
44. Salvador P R, Xu K G. Electric field modified Bunsen flame with variable anode placement. Journal of Thermophysics and Heat Transfer, 2017, 31(4): 956–964

45. Karnani S, Dunn-Rankin D. Detailed characterization of DC electric field effects on small non-premixed flames. Combustion and Flame, 2015, 162(7): 2865–2872
46. Speelman N, Kiefer M, Markus D, et al. Validation of a novel numerical model for the electric currents in burner-stabilized methane-air flames. Proceedings of the Combustion Institute, 2015, 35(1): 847–854
47. Drews A M, Cademartiri L, Chemama M L, et al. Ac electric fields drive steady flows in flames. Physical Review. E, 2012, 86(3): 036314
48. Xiong Y, Park D G, Lee B J, et al. DC field response of one-dimensional flames using an ionized layer model. Combustion and Flame, 2016, 163: 317–325
49. Park S H, Son J W, Park J, et al. Elevated pressure increases the effect of electric fields on ionic wind in methane premixed jet flames. Proceedings of the Combustion Institute, 2021, 38(4): 6679–6686
50. Ren Y, Cui W, Li S. Electrohydrodynamic instability of premixed flames under manipulations of DC electric fields. Physical Review E, 2018, 97(1–1): 013103
51. Wisman D L, Marcum S D, Ganguly B N. Electrical control of the thermodiffusive instability in premixed propane-air flames. Combustion and Flame, 2007, 151(4): 639–648
52. Wisman D, Marcum S, Ganguly B. Electric field induced dissociative recombination at the base of pre-mixed hydrocarbon/air flames. In: 43rd AIAA/ASME/SAE/ASEE Joint Propulsion Conference & Exhibit, Virginia, USA, 2007
53. Wisman D, Ryan M, Carter C, et al. OH PLIF measurements in a low electric field perturbed CH_4/air flame. In: 46th AIAA Aerospace Sciences Meeting and Exhibit, Virigina, USA, 2008
54. Park D G, Chung S H, Cha M S. Dynamic responses of counterflow nonpremixed flames to AC electric field. Combustion and Flame, 2018, 198: 240–248
55. Won S H, Cha M S, Park C S, et al. Effect of electric fields on reattachment and propagation speed of tribrachial flames in laminar coflow jets. Proceedings of the Combustion Institute, 2007, 31(1): 963–970
56. Kim M K, Ryu S K, Won S H, et al. Electric fields effect on liftoff and blowoff of nonpremixed laminar jet flames in a coflow. Combustion and Flame, 2010, 157(1): 17–24
57. Ren Y, Li S, Cui W, et al. Low-frequency AC electric field induced thermoacoustic oscillation of a premixed stagnation flame. Combustion and Flame, 2017, 176: 479–488
58. Ren Y, Cui W, Pitsch H, et al. Experimental and numerical studies on electric field distribution of a premixed stagnation flame under DC power supply. Combustion and Flame, 2020, 215: 103–112
59. Tran M V, Cha M S. Time evolution of propagating nonpremixed flames in a counterflow, annular slot burner under AC electric fields. Proceedings of the Combustion Institute, 2017, 36(1): 1421–1430
60. Tran M V, Cha M S. Propagating nonpremixed edge-flames in a counterflow, annular slot burner under DC electric fields. Combustion and Flame, 2016, 173: 114–122
61. Duan H, Wu X, Zhang C, et al. Experimental study of lean premixed $CH_4/N_2/O_2$ flames under high-frequency alternating-current electric fields. Energy & Fuels, 2015, 29(11): 7601–7611
62. Meng X, Wu X, Kang C, et al. Effects of direct-current (DC) electric fields on flame propagation and combustion characteristics of premixed $CH_4/O_2/N_2$ flames. Energy & Fuels, 2012, 26(11): 6612–6620
63. Vorontsov S S, Ganeev O V, Tretyakov P K, et al. Dynamics of the laminar flame front of a homogeneous propane-air mixture with a pulsed-periodic action of an electric field. Combustion, Explosion, and Shock Waves, 2009, 45(5): 530–533
64. Volkov E N, Kornilov V N, de Goey L P H. Experimental evaluation of DC electric field effect on the thermoacoustic behaviour of flat premixed flames. Proceedings of the Combustion Institute, 2013, 34(1): 955–962
65. Kim M K, Chung S H, Kim H H. Effect of AC electric fields on the stabilization of premixed Bunsen flames. Proceedings of the Combustion Institute, 2011, 33(1): 1137–1144
66. Lee S M, Park C S, Cha M S, et al. Effect of electric fields on the liftoff of nonpremixed turbulent jet flames. IEEE Transactions on Plasma Science, 2005, 33(5): 1703–1709
67. Saito M, Arai T, Arai M. Control of soot emitted from acetylene diffusion flames by applying an electric field. Combustion and Flame, 1999, 119(3): 356–366
68. Chien Y C, Dunn-Rankin D. Electric field induced changes of a diffusion flame and heat transfer near an impinging surface. Energies, 2018, 11(5): 1235
69. Cessou A, Varea E, Criner K, et al. Simultaneous measurements of OH, mixture fraction and velocity fields to investigate flame stabilization enhancement by electric field. Experiments in Fluids, 2012, 52(4): 905–917
70. Altendorfner F, Kuhl J, Zigan L, et al. Study of the influence of electric fields on flames using planar LIF and PIV techniques. Proceedings of the Combustion Institute, 2011, 33(2): 3195–3201
71. Kim G T, Park D G, Cha M S, et al. Flow instability in laminar jet flames driven by alternating current electric fields. Proceedings of the Combustion Institute, 2017, 36(3): 4175–4182
72. Wang Y, Nathan G J, Alwahabi Z T, et al. Effect of a uniform electric field on soot in laminar premixed ethylene/air flames. Combustion and Flame, 2010, 157(7): 1308–1315
73. Tretyakov P K, Tupikin A V, Denisova N V, et al. Laminar propane-air flame in a weak electric field. Combustion, Explosion, and Shock Waves, 2012, 48(2): 130–135
74. Park D G, Chung S H, Cha M S. Visualization of ionic wind in laminar jet flames. Combustion and Flame, 2017, 184: 246–248
75. Butterworth T D, Cha M S. Electric field measurement in electric-field modified flames. Proceedings of the Combustion Institute, 2021, 38(4): 6651–6660
76. Park D G, Choi B C, Cha M S, et al. Soot reduction under DC electric fields in counterflow non-premixed laminar ethylene flames. Combustion Science and Technology, 2014, 186(4–5): 644–656
77. Vatazhin A B, Golentsov D A, Likhter V A. Soot extraction from a laminar hydrocarbon flame by means of an electric field. Fluid Dynamics, 2005, 40(2): 172–178
78. Prikhod'ko N G. Influence of the electric field on the soot formation in the flame at a low pressure. Journal of Engineering Physics and Thermophysics, 2010, 83(1): 171–178
79. Zake M, Turlajs D, Purmals M. Electric field control of NO_x formation in the flame channel flows. Global NEST Journal, 2000, 2

(1): 99–108

80. Zake M, Barmina I, Turlajs D. Electric field control of polluting emissions from a propane flame. Global NEST Journal, 2001, 3(2): 95–108
81. Starikowskii A, Skoblin M, Hammer T. Influence of weak electric fields on the flame structure. In: 2008 17th International Conference on Gas Discharges and Their Applications, Cardiff, UK, 2008
82. Kuhl J, Seeger T, Zigan L, et al. On the effect of ionic wind on structure and temperature of laminar premixed flames influenced by electric fields. Combustion and Flame, 2017, 176: 391–399
83. Hammer T, Lins G, Branston D W, et al. Electric field effects for combustion control–optimized geometry. In: 28th International Conference on Phenomena in Ionized Gases, Prague, Czech Republic, 2007
84. Vega E V, Shin S S, Lee K Y. NO emission of oxygen-enriched $CH_4/O_2/N_2$ premixed flames under electric field. Fuel, 2007, 86(4): 512–519
85. Zhang Y, Wu Y, Yang H, et al. Effect of high-frequency alternating electric fields on the behavior and nitric oxide emission of laminar non-premixed flames. Fuel, 2013, 109: 350–355
86. Xiong Y, Park D G, Cha M S, et al. Effect of buoyancy on dynamical responses of coflow diffusion flame under low-frequency alternating current. Combustion Science and Technology, 2018, 190(10): 1832–1849
87. Xiong Y, Cha M S, Chung S H. AC electric field induced vortex in laminar coflow diffusion flames. Proceedings of the Combustion Institute, 2015, 35(3): 3513–3520
88. Arefyev K Y, Krikunova A I, Panov V A. Complex effect of electric and acoustic fields on air-methane flame blow-off characteristics. High Temperature, 2019, 57(6): 909–915
89. Cha M S, Lee Y. Premixed combustion under electric field in a constant volume chamber. IEEE Transactions on Plasma Science, 2012, 40(12): 3131–3138
90. Belhi M, Domingo P, Vervisch P. Direct numerical simulation of the effect of an electric field on flame stability. Combustion and Flame, 2010, 157(12): 2286–2297
91. Yoon S H, Seo B, Park J, et al. Edge flame propagation via parallel electric fields in nonpremixed coflow jets. Proceedings of the Combustion Institute, 2019, 37(4): 5537–5544
92. van den Boom J D B J, Konnov A A, Verhasselt A M H H, et al. The effect of a DC electric field on the laminar burning velocity of premixed methane/air flames. Proceedings of the Combustion Institute, 2009, 32(1): 1237–1244
93. Wang J, Li Y, Xia H, et al. Effect of hydrogen enrichment and electric field on lean CH_4/air flame propagation at elevated pressure. International Journal of Hydrogen Energy, 2019, 44(30): 15962–15972
94. Li Y, Wang J, Xia H, et al. Effect of DC electric field on laminar premixed spherical propagation flame at elevated pressures up to 0.5 MPa. Combustion Science and Technology, 2018, 190(11): 1900–1922
95. Li C, Wu X, Li Y, et al. Deformation study of lean methane-air premixed spherically expanding flames under a negative direct current electric field. Energies, 2016, 9(9): 738
96. Scarano F. Tomographic PIV: principles and practice. Measurement Science & Technology, 2013, 24(1): 012001
97. Meyer T R, Halls B R, Jiang N, et al. High-speed, three-dimensional tomographic laser-induced incandescence imaging of soot volume fraction in turbulent flames. Optics Express, 2016, 24(26): 29547–29555
98. Halls B R, Hsu P S, Jiang N, et al. kHz-rate four-dimensional fluorescence tomography using an ultraviolet-tunable narrowband burst-mode optical parametric oscillator. Optica, 2017, 4(8): 897–902
99. Liu H, Shui C, Cai W. Time-resolved three-dimensional imaging of flame refractive index via endoscopic background-oriented Schlieren tomography using one single camera. Aerospace Science and Technology, 2020, 97: 105621